Available online at www.sciencedirect.com
ScienceDirect
Ceramics International 37 (2011) 3253–3263
CERAMICS INTERNATIONAL
www.elsevier.com/locate/ceramint

The effect of glucose on the formation of the nanocrystalline transition alumina phases

Zoran Obrenović [a,b], Marija Milanović [c], Ružica R. Djenadić [d], Ivan Stijepović [c], Konstantinos P. Giannakopoulos [e,1], Mitar Perušić [a], Ljubica M. Nikolić [c,*]

[a] Faculty of Technology, University of East Sarajevo, Zvornik, Republic of Srpska, Bosnia and Herzegovina
[b] Alumina factory „Birač", Zvornik, Republic of Srpska, Bosnia and Hercegovina
[c] Department of Materials Engineering, Faculty of Technology, University of Novi Sad, Novi Sad, Serbia
[d] Nanoparticle Process Technology, Department of Engineering Sciences and CeNIDE, University Duisburg–Essen, Duisburg, Germany
[e] Institute of Materials Science, NCSR "Demokritos", Athens, Greece

Received 10 March 2011; received in revised form 18 May 2011; accepted 23 May 2011
Available online 30 May 2011

Abstract

Series of alumina powders were synthesized starting from sodium aluminate solution prepared from Bayer liquor. The neutralisation of sodium aluminate solution was performed with the use of sulphuric acid. The influence of glucose as a non-surfactant additive on the structure of alumina powders at moderate pH was investigated. The results show that the properties of the powders are influenced by the initial pH value of the solution, as well as the duration of the neutralisation step. High pHs lead to the formation of powders with heterogeneous structure with bayerite as a dominant phase, which during calcinations converts to η-alumina with high surface area. Addition of glucose to the starting aluminate solution leads to the formation of nanocrystalline boehmite with estimated average crystallite size less than 3 nm and high surface area (above 300 m^2/g). After calcinations, boehmite transforms to γ-alumina. The results have shown that during the heat treatment, structural transformations proceeded simultaneously with the significant changes in the textural properties of the obtained mesoporous γ- and η-alumina powders.

Keywords: Bayer liquor; Glucose; η-Alumina; γ-Alumina; Nanocrystalline; Surface area

1. Introduction

In the last decade, a great research effort was engaged in the exploration of transition alumina phases from both a fundamental and a practical point of view [1–7]. The transition (active) phases of alumina are metastable polymorphs of aluminium oxide formed through the thermal dehydration of aluminium trihydroxide (bayerite and gibbsite) and aluminium oxyhydroxide (boehmite or pseudoboehmite) in the temperature range of 230–1100 °C [1,7]. These oxide phases, especially γ- and η-alumina, have very diverse possibilities of application in various catalytic processes, as absorbents, membranes, support for noble metals etc. which strongly depends on their structural characteristics such as average crystallite size, surface area, pore volume and pore size distribution. A lot of scientific effort has been devoted to develop optimal methods and conditions for obtaining these transition alumina phases with a desirable microstructure. These materials are generally prepared by the thermal decomposition of well-crystallised hydroxides or via precipitation of colloidal gels [7,8]. The final structure of alumina phases is influenced not only by the synthesis conditions but also by the subsequent thermal treatment.

An inexpensive and non-toxic sodium aluminate solution from Bayer liquor [9] was chosen in this work as a starting material for synthesis of aluminium hydroxide and active alumina phases. The neutralisation of sodium aluminate solution was performed with the use of sulphuric acid in order to avoid the complex procedure of pH adjustment of the solution [10–12]. In contrast to the classical Bayer process where the main product is gibbsite, in this work by the neutralisation of sodium aluminate solution with sulphuric acid

* Corresponding author at: University of Novi Sad, Department of Materials Engineering, Faculty of Technology, Bulevar cara Lazara 1, Novi Sad, Serbia, Tel.: +381 21 485 3758; fax: +381 21 450 413.
E-mail address: ljunik@uns.ac.rs (L.M. Nikolić).
[1] Currently at: Institute of Microelectronics.

0272-8842/$36.00
doi:10.1016/j.ceramint.2011.05.120

and with suitable adjustment of process parameters, we have shown that it is possible to obtain other phases as well (bayerite, boehmite, etc.). Gibbsite and bayerite usually consist of large crystallites with particles on the micrometer scale and with a wide size distribution. One of the ways to control the microstructure (narrow size distribution, mesoporosity, etc.) of alumina phases is the use of various anionic, non-ionic and cationic surfactants in aqueous or in organic solvents [6,13–15]. On the other hand, surfactant removal represents a critical step in the preparation of suitable microstructure and is probably even more important than the synthesis itself, because of the strong possibility for interaction between the surfactant and the alumina which leads to the structural collapse [1,16,17]. In this work, we have investigated the effect of glucose as an organic non-surfactant on tailoring the morphological characteristics of the starting aluminium trihydroxide and the aluminium oxyhydroxide powders, in order to obtain transition alumina phases with similar or improved morphology (crystallites on nanometer scale, narrow particle size and pore size distribution, porosity, etc.).

One of the main aims of this work was to focus also on the control of porosity. There is a limited amount of available data related to the usage of glucose for adjustment of porosity in the alumina phases. However, Xu et al. [18] showed that the presence of glucose in alkoxide solution resulted in the formation of mesoporous amorphous alumina with a high surface area, only after heating at 600 °C. The obtained alumina remained amorphous until 800 °C, when it was transformed to γ-alumina, with a large decrease of surface area. Therefore, in this work, glucose was washed out before any thermal treatment of the powders, so that the collapse of the microstructure can be avoided in the process of the removal of the organic residuals during calcinations.

In order to elucidate the effect of glucose, samples without glucose were synthesized under the same conditions.

2. Experimental

2.1. Synthesis procedure

Transition alumina phases were obtained from aluminium trihydroxide (AH) or aluminium oxohydroxide (AOH) precursors which are synthesized by hydrolysis of diluted sodium aluminate solution (Bayer liquor) that had a concentration of [NaOH] = 0.82 M, [Al(III)] = 0.52 M and pH value of 12 adjusted with 1 M sulphuric acid. The neutralisation procedure was carried out during stirring at 70 °C until pH values decreased to about 10.8. The obtained white precipitate was separated by vacuum filtration. The sulphuric acid was added into the remaining liquid phase (having pH about 10.8) until its pH value further went down to 9.5. The same procedure was used to separate the white precipitate from the liquid phase. Neutralisation procedures were performed very carefully during 30 and 120 min. Obtained powders were washed with distilled water to remove residual ions. After that, powders were dried at 120 °C for 3 h. Dried samples were heated in atmospheric conditions at 500 °C for 3 h with a heating rate of 5 °C/min. In order to investigate the effect of glucose on the morphological characteristics of the finally obtained alumina powders, glucose was added in the sodium aluminate solution with molar ratio of glucose/Al^{+3} being 1/10. Alumina powders prepared with glucose were synthesized using the same procedure as previously described. Sample notations and some conditions of their preparation are given in Table 1. The samples obtained without glucose are marked as ATH-*x* and powders prepared with glucose are marked as ATH-*x*G (where *x* = 1, 2, 3, 4 represents the number of the sample).

Table 1
Sample notation and conditions of their preparation.

Without glucose	With glucose	Solution pH range	Neutralisation time (min)
ATH-1	ATH-1G	12–10.8	30
ATH-2	ATH-2G	10.8–9.5	30
ATH-3	ATH-3G	12–10.8	120
ATH-4	ATH-4G	10.8–9.5	120

2.2. Characterisation techniques

The structural changes caused during the preparation and the thermal treatment of powders were studied by Fourier transformed infrared (FT-IR) spectroscopy and X-ray powder diffraction (XRD). The morphology and the microstructure of the samples were additionally examined by scanning electron microscopy (SEM) and transmission electron microscopy (TEM). FT-IR measurements were performed using a Nicolet-Nexsus 670 FT-IR spectrophotometer. The XRD patterns of the as-synthesized and heat treated powders were collected on a PANalytical X'Pert PRO instrument using Cu-Kα radiation with a wavelength 0.15406 nm and a step of 0.03°/s. The microstructure and morphology of the samples were analyzed using a JEOL JSM 6460 LV scanning electron microscope and a Philips CM20 transmission electron microscope operating at 200 kV, equipped with an energy-dispersive X-ray spectroscopy tool (EDS) and capable of performing the selected area electron diffraction (SAED). Nitrogen adsorption/desorption isotherms were measured on a Quantachrom Autosorb-3B instrument and the specific surface area of the samples was calculated using the BET method. The pore size distribution (PSD) was derived from the desorption branches of the isotherms using the BJH method. The microporosity was estimated using the *t*-plot method.

3. Results and discussion

3.1. The as-synthesized powders

3.1.1. The phase identification from FT-IR spectroscopy

It is well known that gibbsite and bayerite, as two polymorphic forms of aluminium hydroxide, $Al(OH)_3$, have very similar structures, which makes their identification more difficult that still represents a hot issue among researchers [19–21]. These polymorphs have layered structures, where

each sheet consists of double layer of OH groups with Al^{+3} cations occupying two thirds of the octahedral interstices within the layers [21,22]. The main differences between these two polymorphs are in the stacking sequence of the layers (interlayer hydrogen bonds) and the position of OH groups between them (intralayer hydrogen bonds). Unlike bayerite, each double layer in gibbsite is positioned in such a way that the upper and lower neighbouring layers have their hydroxyl groups directly opposite each other and not in the position of the closest packing. This type of layer structure explains the perfect cleavage of gibbsite parallel to the basal plane. The Al–O frame within a sheet is very similar in both phases. From a structural perspective, the most widely used crystal structure phase identification of aluminium hydroxide is based on X-ray diffraction, thus leading to poor characterization of the hydroxyl groups [23]. Determination of the position of the hydroxyl groups and thus more complete structural analysis of these phases can be achieved with the use of spectroscopic methods and one of them is FT-IR spectroscopy. However, the application of this method is quite difficult because both of these alumina phases have prominent –OH stretching and bending modes associated with the interlayer hydrogen bonds which have very similar frequencies. It is worth noticing that there are diverse data related to the position of characteristic stretching modes (which appear at a high wavenumber region) and the corresponding deformation modes of bayerite, gibbsite and even boehmite (in a region of low wavenumbers) [24].

The FT-IR spectra of the as-synthesized ATH-*x* and ATH-*x*G samples are shown in Fig. 1a and b, respectively. It is important to mention that gibbsite and bayerite OH groups have two distinctive types of vibrations with different modes: the hydroxyl stretching frequencies that show a pronounced blue shift, while the hydroxyl deformation mode shows a pronounced red shift. According to the literature data for gibbsite [25], hydroxyl stretching modes appear at about 3617, 3520, 3428 and 3380 cm^{-1} wavenumbers, while the hydroxyl deformation modes appear at 1060, 1024, 980, 916 cm^{-1}. Low-frequency infrared absorption vibrations at about 625, 585, 560, 522, 452, and 423 cm^{-1} could be due to the Al–O–Al vibration bands. Considering structural differences between gibbsite and bayerite, there are distinct differences in the hydroxyl stretching bands between gibbsite (3617–3364 cm^{-1}) and bayerite (3664–3420 cm^{-1}), with the peaks for the latter being systematically shifted to higher wavenumbers [22,26].

The most pronounced bands in the vibration spectrum are the hydroxyl stretching modes, completely separated from all other modes. The characteristic Al–O vibrations are shifted towards the smaller wavenumbers (900–400 cm^{-1}) where the effect of OH-group vibrations is very pronounced. According to the shape and position of stretching Al–OH vibration modes in the FT-IR spectra (Fig. 1a) and taking into account the conditions of synthesis of ATH-*x* samples (Table 1), it can be assumed that bayerite is dominant phase in ATH-1 and ATH-2 powders. For samples ATH-3 and ATH-4 the red shift of stretching Al–OH bands is obvious that indicates the possible occurrence of gibbsite phase in these powders. The band at

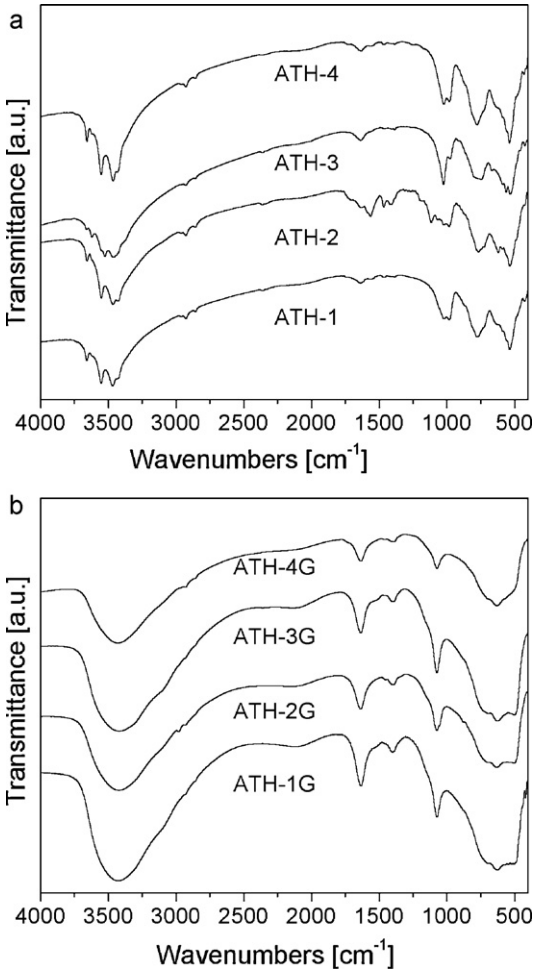

Fig. 1. FT-IR spectra of the as-synthesized alumina powders: (a) ATH-*x* and (b) ATH-*x*G.

about 1640 cm^{-1} is characteristic for the bending mode of the adsorbed water and this band is the most pronounced in the powder ATH-2; this could indicate the higher surface area of this sample in comparison to other powders. The presence of boehmite in these samples (especially in the ATH-2) is confirmed with the widening of the band centred at about 1640 cm^{-1} and wide band between 1113 and 970 cm^{-1}.

Based on the large differences between the FT-IR spectra of samples obtained with glucose, ATH-*x*G (Fig. 1b), and those corresponding to samples obtained without glucose, ATH-*x* (Fig. 1a), one can conclude that the addition of glucose in the sodium aluminate solution affects the mechanisms of nucleation and growth of particles, as well as the phase composition of the as-synthesized powders. These differences are very pronounced in all spectra regions such as the –OH stretching region (3800–2500 cm^{-1}), H–O–H bending region (1700–1600 cm^{-1}) and the –OH bending region (1200–700 cm^{-1}). Despite the different conditions of their preparation, the FT-IR spectra for all ATH-*x*G powders have very similar characteristic bands. In contrast to the ATH-*x*, ATH-*x*G as-synthesized powders have only one wide band centred at about 3440 cm^{-1} which is attributed to the O–H stretching vibration. This band dominates this region and prevents the observation of the features corresponding to the structural OH groups. The band

attributed to the bending vibration of adsorbed water molecules at 1640 cm^{-1} is also quite pronounced in these spectra. In addition, three bands in FT-IR spectra of ATH-*x*G powders can be observed, indicating that all powders consist of the boehmite phase. The weak band that occurred at about 1380 cm^{-1} comes from the vibration of surface –OH groups, the hydroxyl deformation mode is noticed at 1070 cm^{-1} and the strong band centred at 635 cm^{-1} is related to the Al–O stretching vibrations [27,28]. Well defined bands attributed to the different types of –OH and H–O–H vibrations of absorbed water may indicate well developed specific surface areas of as-synthesized ATH-*x*G powders.

3.1.2. The phase identification from XRD

XRD patterns of ATH-x and ATH-xG as-synthesized powders are shown in Fig. 2. It is well known that gibbsite is common product in the classical Bayer process that has been obtained from sodium aluminate solution. Despite the differences in process parameters, such as pH and duration of neutralisation, the XRD patterns of ATH-x samples are very similar (Fig. 2a) and bayerite (ICDD Card No. 20-0011) was identified as a dominant phase. Furthermore, in the XRD pattern of the ATH-2 sample a very weak boehmite peak appears (ICDD Card No. 13-083) (shown in the corresponding SEM image, Fig. 3b). There exist also two phases in ATH-3 and ATH-4 powders. In addition to bayerite, the phase gibbsite appears also (ICDD Card No. 33-0018). The structural similarities of these two phases affect the appearance of their reflections at very close diffraction angles so they are very difficult to distinguish. The presence of gibbsite was confirmed by the appearance of its characteristic peak at 18.3° that overlaps with the characteristic peak of bayerite at 18.8° (inset in Fig. 2a). The characteristic peak of gibbsite is more pronounced in the sample ATH-3 than in ATH-4, which indicates the higher gibbsite quantity in the starting powder. It is worth mentioning that all experimental conditions performed in synthesis of ATH-*x* samples are favourable for obtaining bayerite as the dominant phase in ATH-*x* powders. Since diluted solutions of sodium-aluminate have been used for obtaining AH and AOH phases, it is reasonable to assume that these solutions composed of relatively large, Al(III)-poly-condensed structures. Addition of sulphuric acid leads to the condensation of polymeric species, through the OH groups, and formation of nuclei of bayerite. Increased neutralisation time of sodium aluminate solution, from 30 to 120 min (at constant pH, Table 1) leads to the formation of gibbsite phase together with bayerite, samples ATH-1 and ATH-3. However, the neutralisation of the sodium aluminate solution at lower pH values (at the same neutralisation time, Table 1) leads to a reduction of gibbsite fraction, sample ATH-4.

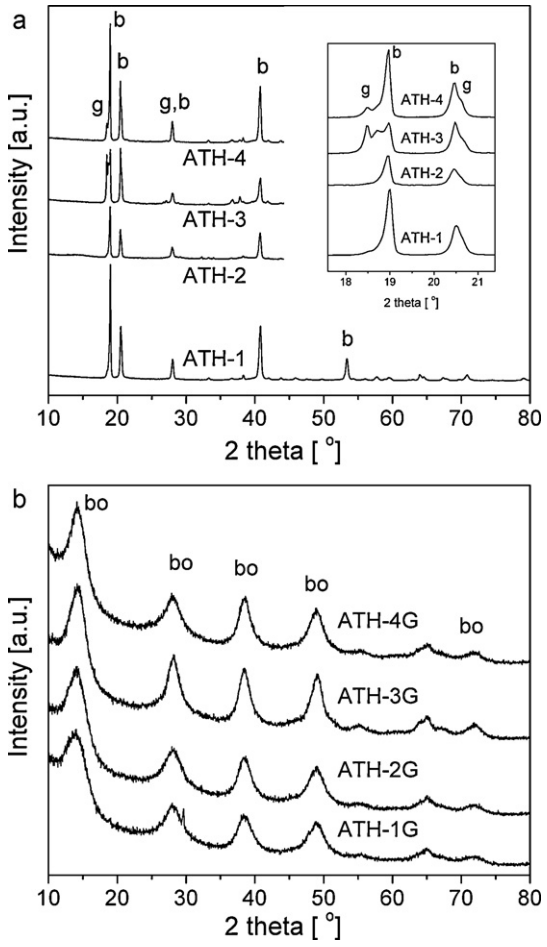

Fig. 2. XRD patterns of the as-synthesized alumina powders: (a) ATH-*x* (inset shows the presence of gibbsite in ATH-3 and ATH-4 samples) and (b) ATH-*x*G (b – bayerite, g – gibbsite, bo – boehmite).

XRD patterns of ATH-xG powders confirm that all as-prepared powders are pure boehmite phase, Fig. 2b. Namely, the addition of glucose to the starting aluminate solution has led to a rather unexpected phenomenon that, in spite differences in pH values and neutralisation time, all as-synthesized ATH-*x*G powders are single phased, nanocrystalline boehmite. These findings are in accordance with previously discussed FT-IR results, Fig. 1b. Previous remarks indicate that the presence of glucose in the sodium aluminate solution influences the mechanism of nucleation and growth of boehmite. Glucose, as non-surfactant, exists in several isomeric forms in the alluminate solution with characteristic –OH groups in *trans* conformation. Through these –OH groups, glucose is probably bound to the polymeric aluminate species, forming weak Al-complexes, thus blocks active sites for nucleation of AH phases and promotes formation of AOH nuclei, i.e. boehmite. In the XRD patterns of as-synthesized ATH-*x*G powders the characteristic peaks of glucose are not observed indicating that glucose was removed during washing of powders.

3.1.3. The microstructural analysis by SEM

Microstructural analysis was performed using SEM and shows different morphology of bayerite crystals as the dominant phase in as-synthesized ATH-*x* powders, Fig. 3. It is well known that the morphology of bayerite crystals depends on the preparation method and the synthesis conditions [28,29]. In the ATH-1 powder two morphologies of bayerite crystals were found: long rods with flat irregular surfaces and agglomerated plate-like crystals, Fig. 3a. The ATH-2 powder is composed of long conical bayerite crystals and very fine and

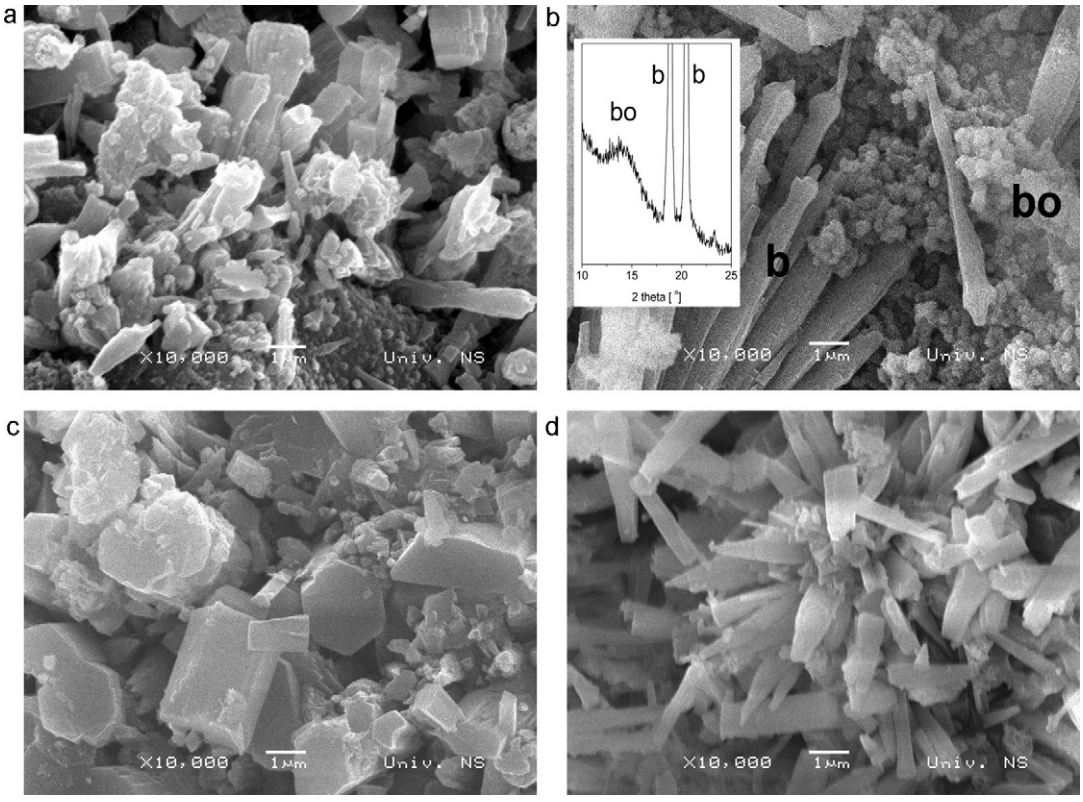

Fig. 3. SEM micrographs of the as-synthesized alumina powders: (a) ATH-1, (b) ATH-2, (c) ATH-3 and (d) ATH-4 (bo – boehmite, b – bayerite).

small boehmite crystallites, Fig. 3b. As-synthesized ATH-3 powder (Fig. 3c) contains rod-shaped forms of bayerite and large hexagonal crystals of gibbsite with sharp edges and flat surfaces. Powder ATH-4 consists of well defined rod-shaped bayerite crystals that are agglomerated and at high resolution these agglomerates consist of plates. These features may be explained by the pH dependence of growth habits: rods are obtained for high pH values, while plates seem to grow at lower pH values. Thus, the decrease of pH during the synthesis leads to the successive formation of different pH-dependant crystallite shapes [20,29–31].

In Fig. 4 SEM micrographs of ATH-*x*G as-synthesized powders are shown; they support further the influence of the glucose addition on the phase composition and morphology of these powders. Compared to the powders obtained without addition of glucose, ATH-*x* (Fig. 3), it is obvious that ATH-*x*G powders consist of fine agglomerated nanocrystalline boehmite. The degree of agglomeration and size of agglomerates depend on the process parameters such as pH and duration of neutralisation.

3.1.4. The specific surface area from BET

The specific surface areas of as-synthesized powders without glucose (ATH-*x*) and with glucose (ATH-*x*G) given in Table 2, impose some important remarks that are consistent with previously discussed results. First of all, ATH-2 sample has the highest surface area (50 m^2/g) compared to the other ATH-*x* powders (with values up to 21 m^2/g). Subsequently, the generally low values of surface area of ATH-*x* powders are the consequence of their morphology which mostly consists of larger crystals of bayerite (samples ATH-1, ATH-2) or a mixture of bayerite and gibbsite crystals (sample ATH-3 and ATH-4) and this is consistent with the SEM results, Fig. 3. On the other hand, it is important to highlight the large values of surface area of powders obtained with glucose, ATH-*x*G (above 300 m^2/g) as compared to surface area of powders obtained under the same conditions but without addition of glucose. These differences are due to different phase composition, size of primary crystallites as well as pore size and morphology. Since the crystalline alumina samples usually have a lower surface area than the amorphous ones [31] the decrease in surface area of ATH-*x* powders could be a consequence of the higher crystallization and growth of the aluminium hydroxide. The addition of glucose leads to the formation of pure nanocrystalline boehmite with average crystallite size of 2–3 nm in contrast to the as-synthesized ATH-*x* powders which are composed mostly of the bayerite phase and less of a fraction of gibbsite or boehmite, depending on the synthesis parameters.

Table 2
BET surface area (S_{BET}) of the as-synthesized powders.

Powders without glucose	S_{BET} [m^2/g]	Powders with glucose	S_{BET} [m^2/g]
ATH-1	21	ATH-1G	354
ATH-2	50	ATH-2G	391
ATH-3	17	ATH-3G	304
ATH-4	20	ATH-4G	313

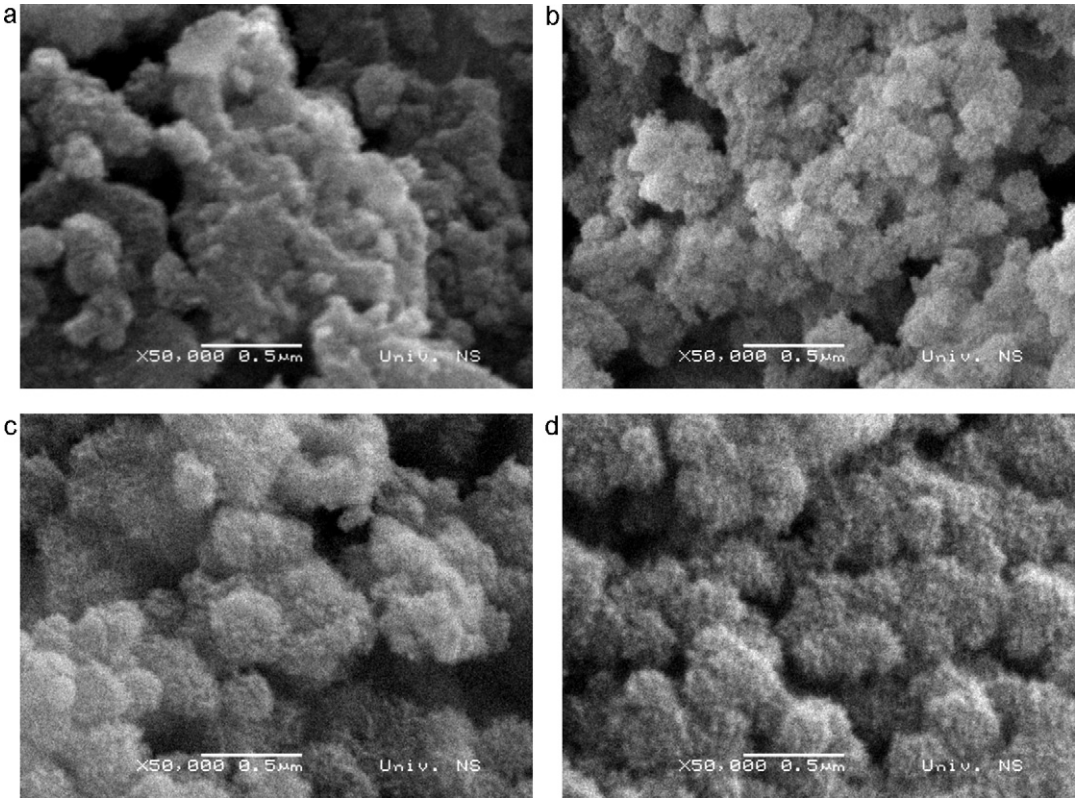

Fig. 4. SEM micrographs of the as-synthesized samples: (a) ATH-1G, (b) ATH-2G, (c) ATH-3G and (d) ATH-4G (bo – boehmite, b – bayerite).

The presence of glucose in sodium aluminate solution controls the precipitation process and influences the formation of boehmite crystallites with narrow size distribution indicating that the nucleation step was more favourable than the growth mechanism.

3.2. The heat treated powders

3.2.1. The phase identification from FT-IR spectroscopy

The FT-IR spectra of ATH-*x*/500 and ATH-*x*G/500 samples after heating at 500 °C for 3 h are presented in Fig. 5. As expected, for ATH-*x*/500 powders, the largest spectral changes occurred in the –OH stretching and H–O–H bending regions. During heating, the ATH-*x*/500 samples were subjected to dehydroxylation, followed by the disappearance of the hydroxyl stretching bands and the appearance of the band centred at about 3464 cm^{-1}. This band and the band at approximately 1640 cm^{-1} are common for the stretching and bending modes of adsorbed water, respectively. In addition, two overlapped bands centred at about 800 cm^{-1} and 600 cm^{-1} have appeared in the spectra of all samples that could be attributed to aluminium ions in tetrahedral and octahedral environments [32] which are typical for a transition alumina phases. The FT-IR spectra of ATH-*x*/500 samples, Fig. 5a, indicate that these samples undergo, during heat treatment, phase transformation from bayerite, gibbsite and boehmite to transition alumina phases. The presence of the weak boehmite characteristic band (at around 1143 cm^{-1}) in the sample ATH-2/500 and considerably less in the sample ATH-1/500 indicates the formation of this phase during the dehydroxylation of bayerite. It is obvious that, although the samples were subjected to dehydroxylation under heating, there were no drastic changes in the FT-IR spectra of ATH-*x*G/500 heated samples, in respect to as-synthesized powders, Fig. 5b. The hydroxyl stretching modes of heated ATH-*x*G/500 powders are shifted to the higher wavenumbers (at 3470 cm^{-1}) which could be attributed to decreased distance in hydrogen bonding between adjacent layers. It is worth noticing a very strong and pronounced stretching and bending modes of adsorbed water (at 3470 and 1640 cm^{-1}) which may be due to the large surface area of the powders. In addition, the wide band in the range of different Al–O modes (800–400 cm^{-1}) splits into two bands centred at ~600 and ~800 cm^{-1}, which can be assigned to the Al–O bonding vibration in tetrahedral and octahedral environments respectively, indicating the presence of some of the active phase of alumina.

3.2.2. The phase identification from XRD

XRD patterns of ATH-*x*/500 and ATH*x*-G/500 powders after thermal treatment at 500 °C/3 h are shown in Fig. 6. The as-synthesized powders transformed into the active oxide phases of alumina during heating, mainly the γ- and η-alumina phases. It is reported [14,33,34] that during heating, the bayerite and pseudoboehmite phases transform to η-alumina, whereas gibbsite and boehmite phases transform to γ-transition alumina phase [34,35]. It is also well known [33] that there is a very high structural similarity between these two phases so it is very difficult to rely on their identification using the XRD method

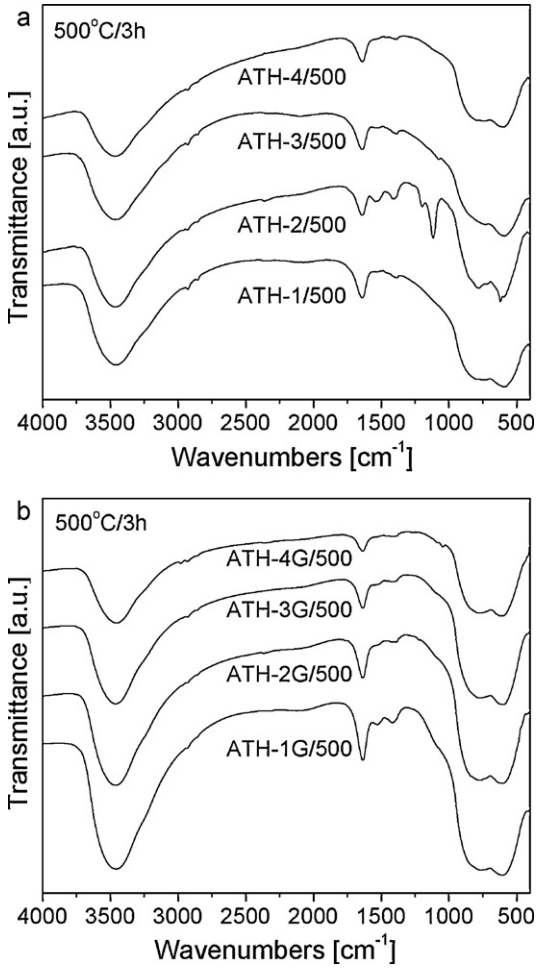

Fig. 5. FT-IR spectra of powders: (a) ATH-*x*/500 and (b) ATH-*x*G/500 after heat treatment at 500°/3 h.

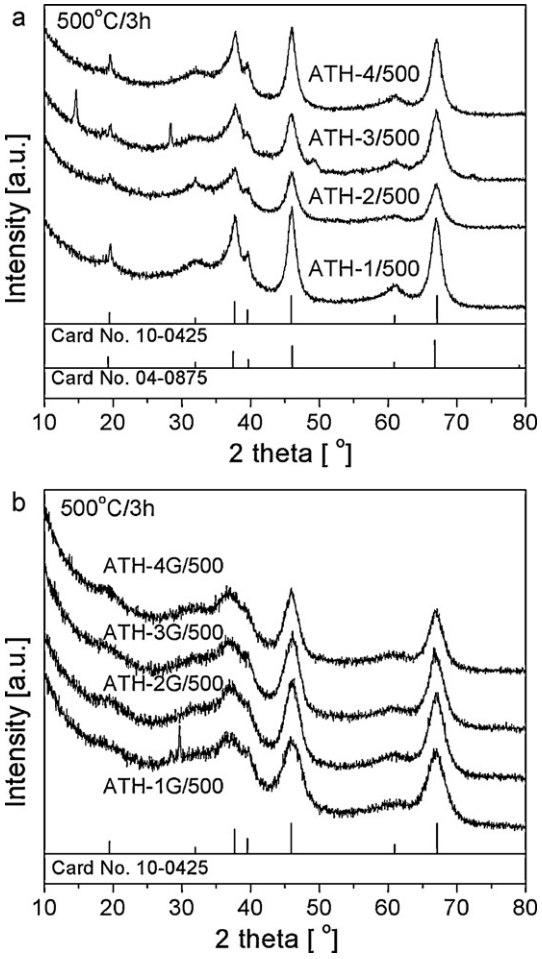

Fig. 6. XRD patterns of powders after heat treatment at 500 °C/3 h: (a) ATH-*x*/500 and (b) ATH-*x*G/500 (ICDD Card No. 10-0425 for γ-alumina; ICDD Card No. 04-0875 for η-alumina).

[36,37]. The transition γ-and η-alumina phases have a spinel-cubic structure with the lattice constants of $a = 0.794$ and 0.790 nm, respectively [38]. However, according to some authors this structure model does not accurately describe the defect structure of γ-alumina and a more accurate description of the structure has been achieved using supercells of the cubic and tetragonal cell [39].

Taking into an account previous consideration, the ATH-*x*/500 powders with a dominant bayerite phase, after the heat treatment, most probably transform to η-alumina (ICDD Card No. 04-0875). The average crystallite sizes of ATH-*x*/500 powders, estimated from Scherrer equation (at $2\theta = 45.8^\circ$ and 66.8°, respectively), are in the range 3.4–4.2 nm. The presence of nanocrystalline boehmite in ATH-2 as-synthesized powder probably had an impact on obtaining the transition phase of alumina with finer particles (average crystallite size is about 2 nm); this is evident in slightly broader diffraction peaks with respect to the peaks of the XRD patterns of the other heated ATH-*x*/500 powders. In addition, the presence of boehmite in as-synthesized ATH-2 powder as well as a significant fraction of gibbsite in as-synthesized ATH-3 and ATH-4 powders affected the phase composition of these powders after heating, so they probably consist of η-alumina and some amount of the γ-phase (ICDD Card No. 10-0425). In the XRD pattern of ATH-3/500 heated powder there are residual boehmite peaks at 2θ of 14.5 and 28.18°, which is probably due to its initial composition and the existence of large gibbsite crystals that impede the phase transformation in the active phase of alumina [33]. The similarity of XRD patterns of ATH-*x*G/500 heated powders, Fig. 6b, indicates their similar phase compositions, which could be attributed to the γ-alumina phase with average crystallite size between 2.2 and 2.7 nm.

3.2.3. The specific surface area from BET

In Fig. 7 there is a typical example of nitrogen adsorption/desorption isotherms and BJH pore size distributions (derived from the desorption branches) of the ATH-1/500 and ATH-1G/500 powders, after heat treatment at 500 °C/3 h. The conventional methods (such as the BJH) for analysis of the adsorption isotherms and the calculation of the pore size distribution can be used only in a certain relative pressure (p/p_0) range and has some constraints [40]. One of these constraints is that it does not take into account the impact of

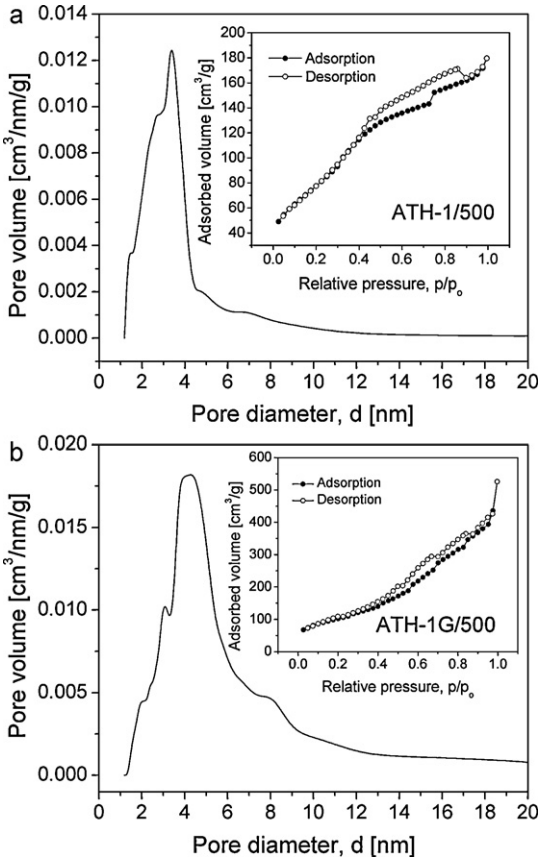

Fig. 7. Nitrogen adsorption/desorption isotherms and corresponding BJH pore size distribution of: (a) ATH-1/500 and (b) ATH-1G/500 powders.

the network of pores, the energy homogeneity of the pore walls, the effects that occur when filling and emptying the pores, etc. Therefore, one should be very careful with the interpretation of results that concern the magnitude and distribution of pores.

Values of the BET surface area, the total pore volume and the micropore surface area (estimated by *t*-plot) of ATH-*x*/500 and ATH-*x*G/500 powders after heat treatment at 500 °C/3 h are given in Table 3. Results obtained using the BET method show that heat treatment has a very pronounced effect on the formation of porosity and on the pore size distribution in ATH-*x*/500 powders. The increase of the surface areas of these

Table 3
BET surface area (S_{BET}), micropore surface area (estimated by a *t*-plot method) and total pore volume of the heated powders.

Sample notation	S_{BET} [m²/g]	Micropore surface area [m²/g]	Pore volume [m³/g]
ATH-1/500	297	163	0.29
ATH-2/500	251	58	0.39
ATH-3/500	300	160	0.29
ATH-4/500	341	203	0.32
ATH-1G/500	379	–	0.82
ATH-2G/500	396	–	1.06
ATH-3G/500	275	–	0.60
ATH-4G/500	2685	–	0.51

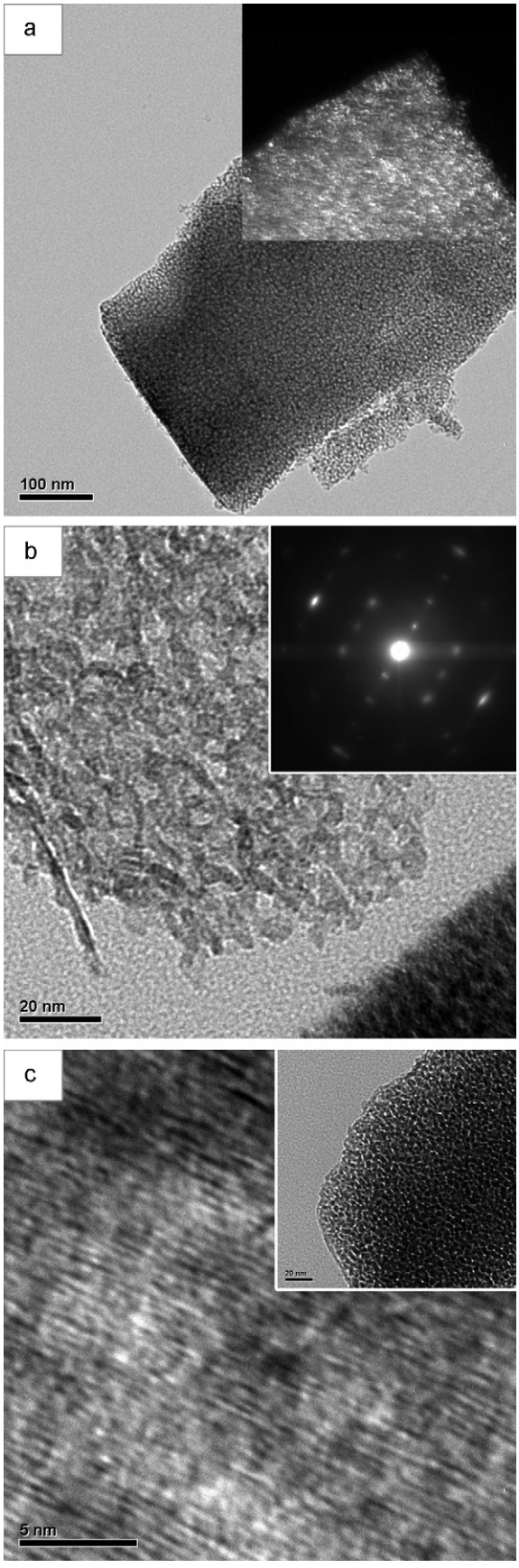

Fig. 8. TEM and HRTEM micrographs of ATH-1/500 powder after heat treatment at 500 °C/3 h.

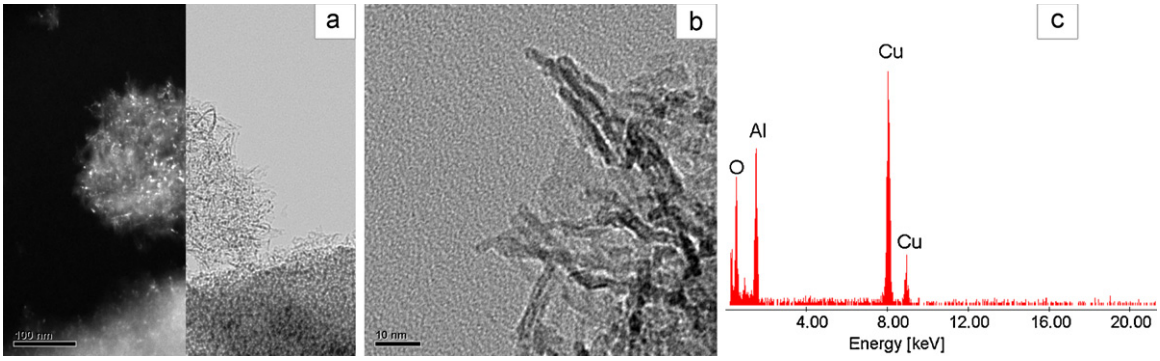

Fig. 9. (a) TEM and (b) HRTEM micrographs of ATH-1G/500 powder after heat treatment at 500 °C/3 h; (c) EDS spectrum of the transition alumina phase, acquired with a Cu TEM holder.

powders after heating is the result of the phase transition of dominant bayerite phase to η-alumina, Tables 2 and 3. A *t*-plot analysis of the adsorption isotherms indicated the presence of microporosity in ATH-*x*/500 powders, Table 3. On the other hand, there is no significant change in the specific surface areas of the ATH-*x*G/500 powders after heat treatment; this is probably caused by the isomorphous transformation of very fine boehmite crystallites (with high specific surface area, Table 2) into nanocrystalline transition alumina. According to *t*-plot analysis, there is no evidence of microporosity in the heat treated powders with glucose. Moreover, the presence of glucose in ATH-*x*G/500 powders has a profound effect on the increase of the pore size, affecting the slight shift of pore size distribution towards higher mesoporosity in respect to ATH-*x*/500 powders, Fig. 7.

3.2.4. The microstructural analysis by TEM

TEM micrographs of ATH-1/500 and ATH-1G/500 powders after heat treatment are presented in Figs. 8 and 9. TEM analysis has shown that investigated samples are polycrystalline porous alumina. It is well documented that aluminium hydroxides and oxyhydroxides undergo an isomorphous transformation to active alumina phase upon heating to 500 °C [1,30]. As a result, the obtained γ- and η-alumina phases can essentially retain the morphology of their parent. These images can confirm the above statement. Fig. 8a and b reflects the shape of the parent bayerite crystal (see Fig. 3a) that during the heat treatment underwent the phase transition to η-alumina with very fine pore sizes in the range 3–6 nm, Fig. 8c. Porosity inside the crystal, formed during the dehydroxylation and the phase transformation, consequently leads to the significant increase in the specific surface area when compared to the as-synthesized ATH-*x* powders, which is consistent with the N_2 adsorption results. TEM analysis confirmed the wide crystallite size distribution in these powders (2–600 nm), Fig. 8a and b. Large crystallites produced the SAED pattern shown in Fig. 8b. Detailed structural information of the alumina phase is revealed by the HRTEM study. The high-resolution image (Fig. 8c) gives a *d* spacing of about 4.6 Å, which matches very well with the crystal plane (1 1 1) of η-alumina. The fact that the fringes are not straight is another indication that the crystal has been affected by the creation of pores.

TEM images of ATH-1G/500 sample (Fig. 9a and b) show significant difference in morphology of the formed porous active alumina in respect to the powders without glucose, caused by the nanocrystalline nature of the starting material (boehmite, see Fig. 4a). Nanocrystalline boehmite, which is formed by addition of glucose to sodium-aluminate solution, during heating, was transformed to very fine polycrystalline material with crystallites between 2 and 8 nm, and a very specific and rough porous appearance, on which one can clearly observe nanometer sized one-dimensional structures. As is well known, boehmite is a type of layered materials, with each layer composed of parallel double chains of AlO_6 octahedra, forming AlOOH layers with the OH groups between them [41]. In our case, the presence of glucose in the starting solution affects the mechanism of nucleation and growth of the AH and AOH particles, by reducing the inclination of interlayer stacking trough hydrogen bonds and favouring the growth of boehmite nanosheets. This specific boehmite structure isomorphously transforms to γ-alumina retaining the lamellar morphology of the parent phase, which is well confirmed by TEM analysis, Fig. 9. It is worth noticing, that in spite of using Bayer liquor as a starting solution, all the obtained powders are pure alumina, which is confirmed by EDS spectra, typical for all samples, Fig. 9c (the Cu peaks are attributed to the TEM holder).

4. Conclusions

The results have shown that the use of inexpensive and non-toxic precursors (sodium aluminate from Bayer liquor, sulphuric acid and glucose) and by careful adjustment of synthesis conditions, it is possible to tailor phase composition and morphology of alumina phases. All powders were synthesized during neutralisation of diluted sodium aluminate solutions with sulphuric acid. Bayerite is a dominant phase in all as-synthesized ATH-*x* powders that are prepared without glucose. Decreased pH value of the starting sodium aluminate solution or extended duration of the neutralisation procedure leads to the formation of less abundant phases of gibbsite and boehmite, along with the bayerite phase. The as-synthesized

ATH-x powders have very small surface areas (below 50 m^2/g) which drastically increase after heat treatment due to the phase transition of bayerite to η-alumina. A *t*-plot analysis has shown the presence of micropores in these samples.

The addition of glucose to the starting aluminate solution has led to a rather unexpected phenomenon, where in spite of differences in pH values and neutralisation times, all as-synthesized ATH-*x*G powders are single phase, nanocrystalline boehmite, with estimated average crystallite size less than 3 nm and a high surface area (from 304 to 391 m^2/g). This indicates that glucose, as a low-cost and environmentally friendly non-surfactant, affects the mechanism of neutralisation reaction resulting in nanocrystalline single phase boehmite formation. The heat treatment of nanocrystalline boehmite powders promotes the transition to an active alumina phase with large surface area and total pore volumes, with a simultaneous increase of the mesopore size.

In a view of the substantially improved microstructural properties of the obtained transition alumina phases, glucose has been proven to be a promising agent for modification and optimisation of the proposed synthesis procedure. One of the additional advantages of this organic agent is the ease in removal completely by water extraction. Future studies will be devoted to possible application of these promising forms of transition alumina.

Acknowledgements

Authors would like to acknowledge the support from the Serbian Ministry of Science, Project No. III45021.

References

[1] Z. Zhang, T.J. Pinnavaia, Mesostructured forms of the transition phases η- and χ-Al_2O_3, Angew. Chem. Int. Ed. 47 (2008) 7501–7504.
[2] J.M. McHale, A. Navrotsky, A.J. Perrotta, Effects of increased surface area and chemisorbed H_2O on the relative stability of nanocrystalline γ-Al_2O_3 and α-Al_2O_3, J. Phys. Chem. B 101 (1997) 603–613.
[3] A.R. Keshavarz, M. Rezaei, F. Yaripour, Nanocrystalline gamma-alumina: a highly active catalyst for dimethyl ether synthesis, Powder Technol. 199 (2010) 176–179.
[4] Y.F. Tang, J. Qi, Z.B. Gu, Z.P. Huang, A.D. Li, Y.F. Chen, Fabrication of uniform porous alumina materials by radio frequency (RF) magnetron sputtering, Appl. Surf. Sci. 254 (2008) 2229–2232.
[5] A.C. Vieira Coelho, G.A. Rocha, P. Souza Santos, H. Souza Santos, P.K. Kiyohara, Specific surface area and structures of aluminas from fibrillar pseudoboehmite, Revista Matéria 13 (2) (2008) 329–341.
[6] N. Žilkova, A. Zukal, J. Čejka, Synthesis of organized mesoporous alumina templated with ionic liquids, Microporous Mesoporous Mater. 95 (2006) 176–179.
[7] J. Čejka, P.J. Kooyman, L. Vesela, J. Rathousky, A. Zukala, High-temperature transformations of organised mesoporous alumina, Phys. Chem. Chem. Phys. 4 (2002) 4823–4829.
[8] C. Marquez-Alvarez, N. Žilkova, J. Perez-Pariente, J. Čejka, Synthesis, characterization and catalytic applications of organized mesoporous aluminas, Catal. Rev. Sci. Eng. 50 (2008) 222–286.
[9] W. Deng, P. Bodart, M. Pruski, B.H. Shanks, Characterization of mesoporous alumina molecular sieves synthesized by nonionic templating, Microporous Mesoporous Mater. 52 (2002) 169–177.
[10] Z. Zhang, R.W. Hicks, T.R. Pauly, T.J. Pinnavaia, Mesostructured forms of γ-Al_2O_3, J. Am. Chem. Soc. 124 (8) (2002) 1592–1593.
[11] Z. Zhang, T.J. Pinnavaia, Mesostructured γ-Al_2O_3 with a lathlike framework morphology, J. Am. Chem. Soc. 124 (41) (2002) 12294–12301.
[12] S. Valange, J.L. Guth, F. Kolenda, S. Lacombe, Z. Gabelica, Synthesis strategies leading to surfactant-assisted aluminas with controlled mesoporosity in aqueous media, Microporous Mesoporous Mater. 35–36 (2000) 597–607.
[13] Y. Liu, D. Ma, X. Han, X. Bao, W. Frandsen, D. Wang, D. Su, Hydrothermal synthesis of microscale boehmite and gamma nanoleaves alumina, Mater. Lett. 62 (2008) 1297–1301.
[14] S.D. Vaidya, N.V. Thakkar, Effect of temperature, pH and ageing time on hydration of rho alumina by studying phase composition and surface properties of transition alumina obtained after thermal dehydration, Mater. Lett. 51 (2001) 295–300.
[15] J.C. Ray, K.S. You, J.W. Ahn, W.S. Ahn, Mesoporous alumina (I): comparison of synthesis schemes using anionic, cationic, and non-ionic surfactants, Microporous Mesoporous Mater. 100 (2007) 183–190.
[16] J Čejka, Organized mesoporous alumina: synthesis, structure and potential in catalysis, Appl. Catal. A 254 (2003) 327–338.
[17] Z.-X. Sun, T.-T. Zheng, Q.-B. Bo, D. Vaughan, M. Warren, Effects of alkali metal ions on the formation of mesoporous alumina, J. Mater. Chem. 18 (2008) 5941–5947.
[18] B. Xu, T. Xiao, Z. Yan, X. Sun, J. Sloan, S.L. Gonzalez-Cortes, F. Alshahrani, M.L.H. Green, Synthesis of mesoporous alumina with highly thermal stability using glucose template in aqueous system, Microporous Mesoporous Mater. 91 (2006) 293–295.
[19] H. Liu, J. Hu, J. Xu, Z. Liu, J. Shu, H.K. Mao, J. Chen, Phase transition and compression behavior of gibbsite under high-pressure, Phys. Chem. Miner. 31 (2004) 240–246.
[20] H. Li, J. Addai-Mensah, J.C. Thomas, A.R. Gerson, The crystallization mechanism of $Al(OH)_3$ from sodium aluminate solutions, J. Cryst. Growth 279 (2005) 508–520.
[21] J.T. Kloprogge, L.V. Duong, B.J. Wood, R.L. Frost, XPS study of the major minerals in bauxite: gibbsite, bayerite and (pseudo-)boehmite, J. Colloid Interface Sci. 296 (2006) 572–576.
[22] R. Demichelis, B. Civalleri, Y. Noel, A. Meyer, R. Dovesi, Structure and stability of aluminium trihydroxides bayerite and gibbsite: a quantum mechanical ab initio study with the CRYSTAL06 code, Chem. Phys. Lett. 465 (2008) 220–225.
[23] J.D. Gale, A.L. Rohl, V. Milman, M.C. Warren, An ab initio study of the structure and properties of aluminium hydroxide: gibbsite and bayerite, J. Phys. Chem. B 105 (2001) 10236–10242.
[24] H.D. Ruan, R.L. Frost, J.T. Kloprogge, Comparison of Raman spectra in characterizing gibbsite, bayerite, diaspore and boehmite, J. Raman Spectrosc. 32 (2001) 745–750.
[25] R.L. Frost, J.T. Kloprogge, S.C. Russell, J.L. Szetu, Vibrational spectroscopy and dehydroxylation of aluminum (oxo)hydroxides: gibbsite, Appl. Spectrosc. 53 (4) (1999) 423–434.
[26] J.T. Kloprogge, H.D. Ruan, R.L. Frost, Thermal decomposition of bauxite minerals: infrared emission spectroscopy of gibbsite, boehmite and diaspore, J. Mater. Sci. 37 (6) (2002) 1121–1129.
[27] Q. Chen, C. Udomsangpetch, S.C. Shen, Y.C. Liu, Z. Chen, X.T. Zeng, The effect of AlOOH boehmite nanorods on mechanical property of hybrid composite coatings, Thin Solid Films 517 (2009) 4871–4874.
[28] S.-L. Wang, C.T. Johnston, D.L. Bish, J.L. White, S.L. Hem, Water-vapor adsorption and surface area measurement of poorly crystalline boehmite, J. Colloid Interface Sci. 260 (2003) 26–35.
[29] G. Lefevre, M. Fedoroff, Synthesis of bayerite (β-$Al(OH)_3$) microrods by neutralization of aluminate ions at constant pH, Mater. Lett. 56 (2002) 978–983.
[30] P. Bai, P. Wu, Z. Yan, X.S. Zhao, A reverse cation–anion double hydrolysis approach to the synthesis of mesoporous γ-Al_2O_3 with a bimodal pore size distribution, Microporous Mesoporous Mater. 118 (2009) 288–295.
[31] P. Bai, P. Wu, Z. Yan, X.S. Zhao, Cation–anion double hydrolysis derived mesoporous γ-Al_2O_3 as an environmentally friendly and efficient aldol reaction catalyst, J. Mater. Chem. 19 (2009) 1554–1563.
[32] M.I.F. Macedo, C.C. Osawa, C.A. Bertran, Sol–gel synthesis of transparent alumina gel and pure gamma alumina by urea hydrolysis of aluminum nitrate, J. Sol-Gel Sci. Technol. 30 (2004) 135–140.

[33] D.B. Tilley, R.A. Eggleton, The natural occurrence of eta-alumina (η-Al_2O_3) in bauxite, Clays Clay Miner. 44 (1996) 658–664.
[34] D. Panias, A. Krestou, Effect of synthesis parameters on precipitation of nanocrystalline boehmite from aluminate solutions, Powder Technol. 175 (2007) 163–173.
[35] T. Tsukada, H. Segawa, A. Yasumori, K. Okada, Crystallinity of bohemite and its effect on the phase transition temperature of alumina, J. Mater. Chem. 9 (1999) 549–553.
[36] C.A. Spitler, S.S. Polack, On the X-ray diffraction patterns of η- and γ-alumina, J. Catal. 69 (1981) 241.
[37] R.-S. Zhou, R.L. Snyder, Structures and transformations mechanism of the η, γ and θ transition aluminas, Acta Crystallogr., Sect. B: Struct. Sci. 47 (1991) 617–630.
[38] J.H. Park, M.K. Lee, C.K. Rhee, W.W. Kim, Control of hydrolytic reaction of aluminum particles for aluminum oxide nanofibers, Mater. Sci. Eng., A 375–377 (2004) 1263–1268.
[39] G. Paglia, Determination of the structure of γ-alumina using empirical and first principles calculations combined with supporting experiments, Ph.D. thesis, Curtin University of Technology, 2004.
[40] J.C. Groen, L.A.A. Peffer, J. Pérez-Ramírez, Pore size determination in modified micro- and mesoporous materials. Pitfalls and limitations in gas adsorption data analysis, Microporous Mesoporous Mater. 60 (2003) 1–17.
[41] Y. Liu, D. Ma, X. Han, X. Bao, W. Frandsen, D. Wang, D. Su, Hydrothermal synthesis of microscale boehmite and gamma nano leaves alumina, Mater. Lett. 62 (2008) 1297–1301.